Published in final edited form as:
Stroke. 2009 June ; 40(6): 2165–2172. doi:10.1161/STROKEAHA.108.540864.

Evaluation of MR derived cerebral oxygen metabolic index in experimental hyperoxic hypercapnia, hypoxia and ischemia

Hongyu An, D.Sc, **Qingwei Liu, B.S**, **Yasheng Chen, D.Sc.**, and **Weili Lin, Ph.D**
Department of Radiology, University of North Carolina at Chapel Hill

Abstract

Background and Purpose—A non-invasive MRI method to measure cerebral oxygen metabolism has the potential to assess tissue viability during cerebral ischemia. The purposes of this study were 1) to validate MR oxygenation measurements across a wide range of global cerebral oxygenation; and 2) to examine the spatiotemporal evolution of oxygen metabolism during focal middle cerebral artery occlusion (MCAO) in rats.

Methods—A group of rats (n=28) under normal, hyperoxic hypercapnia and hypoxia were studied to compare MR measured cerebral oxygen saturation ($O2Sat_{MRv}$) with blood gas oximetry measurements in the jugular vein ($O2Sat_{JV}$) and superior sagittal sinus ($O2Sat_{SSS}$). In a separate group of rats (n=31), MR measured cerebral oxygen metabolic index (MR_COMI) was acquired at multiple time-points during MCAO. Histogram analysis was performed on the normalized MR_COMI (rMR_COMI) to examine evolution of oxygen metabolism during acute ischemia.

Results—Highly linear relationships were obtained between $O2Sat_{MRv}$ and $O2Sat_{JV}$/$O2Sat_{SSS}$ in rats under global cerebral oxygenation alterations. In the focal ischemia study, rMR_COMI values were significantly lower within the areas of eventual infarction than other regions. Moreover, the rMR_COMI values within the ischemic territory decreased with time, concomitant with an increase in the number of voxels with severely impaired oxygen metabolism.

Conclusion—Accurate estimates of $O2Sat_{MRv}$ can be obtained across a broad and physiologically relevant range of cerebral oxygenation. Furthermore, this method demonstrates a dynamic alteration of cerebral oxygen metabolism during acute ischemia in rats.

Keywords

cerebral oxygen metabolism; ischemic stroke; hyperoxic hypercapnia; hypoxia

INTRODUCTION

In vivo quantification of cerebral oxygen metabolism has shown great promise in revealing brain tissue viability during cerebral ischemia. Using sequential positron emission tomography (PET) in a transient middle cerebral artery occlusion (MCAO) primate model, Frykholm et al demonstrated that both cerebral blood flow (CBF) and oxygen extraction fraction (OEF) varied greatly over time with no consistent difference in values between penumbral and the eventually infarcted tissues[1]. In contrast, cerebral metabolic rate of oxygen ($CMRO_2$ = CBF × OEF × arterial oxygen content) values provided a clear demarcation between surviving and dying tissues[1]. Using a transient MCAO (6-hours occlusion) baboon model, Young et al showed that the final infarct region had a significantly lower $CMRO_2$ values compared to the contralateral

Correspondence: Hongyu An, D.Sc., Department of Radiology, 106 Mason Farm Rd., CB#7515, University of North Carolina at Chapel Hill, Chapel Hill, NC 27599. Email: E-mail: hongyuan@med.unc.edu, Telephone: (919) 843-8256, Fax: (919) 843-4456.

hemisphere before reperfusion [2]. Together, these results suggest that $CMRO_2$, which reflects the balance between oxygen delivery (CBF) and demand (OEF), may offer an improved means to assess tissue viability during acute cerebral ischemia [1, 3].

To date, PET has been the method of choice to measure $CMRO_2$. However, PET is invasive, requires an onsite cyclotron, and is not readily accessible at most medical centers especially for acute stroke studies. In addition, an arterial line is required to obtain quantitative measurements, making it impractical for patients receiving tPA. Therefore, an approach capable of providing similar physiological information to that of $CMRO_2$ but without the limitations of PET could dramatically improve accessibility to acute stroke patients. We have previously reported an MR approach to estimate OEF(MR_OEF) and demonstrated MR_OEF similar to that obtained using PET under normo- and hyperoxic hypercapnia [4–6]. However, a direct comparison to a gold standard has not yet been performed. To this end, the first goal of this study was to assess the accuracy of MR_OEF through a direct comparison with blood gas oximetry under a wide range of inhalant oxygen content manipulation. In addition, combining MR_OEF with MR measured CBF, MR measured cerebral oxygen metabolic index (MR_COMI) can be obtained [7, 8]. Although the means through which MR_COMI is derived differs from PET $CMRO_2$, MR_COMI provides similar physiological information to that of PET $CMRO_2$. Therefore, the second goal of our study was to examine the spatiotemporal evolution of MR_COMI during acute experimental focal ischemia in rats.

MATERIALS AND METHODS

Animal Methods

All animal protocols were approved by the Institutional Animal Care and Use Committee. In total, fifty-nine male Long Evans rats, 250 – 350 grams, were studied. Animals were divided into two groups: the global gas manipulation group (Group A, n=28) and the middle cerebral artery occlusion (MCAO) stroke group (Group B, n=31).

Group A was further divided into the calibration Group A1 (n=10) and imaging Group A2 (n=18). All animals were anesthetized with isoflurane (inhaled, 5% induction, and 1.5% maintenance) and mechanically ventilated (Harvard Apparatus, Holliston MA) via a tracheotomy after treatment with pancuronium bromide (0.1 ml/100g). Femoral artery (FA) blood samples were obtained to monitor physiological conditions for all animals. Ventilation rate was set at 50 strokes/minute and tidal volume ranged from 2.5 to 3 ml/stroke to maintain baseline femoral artery PCO_2 within 35–45 mmHg using room air ventilation. The inhaled gas mixture was varied to alter cerebral blood oxygenation: control (room air), hyperoxic hypercapnia (carbogen, 3% CO2 mixed with 97% O2), and moderate (nitrogen/room air=1/2) and severe (nitrogen/room air=2/1) hypoxia. The reduced oxygen content during nitrogen/room air breathing caused a reduction in cerebral O2Sat (hypoxia). On the other hand, gas mixture of O2 and CO2, which was referred to as “carbogen”, have been utilized to increase pCO2, pO2 and cerebral O2Sat [9–12] (hyperoxia hypercapnia).

All animals underwent a series of gas challenges by alternating room air and carbogen or nitrogen/air mixture. A total of 24 control, 5 hypercapnic, 10 moderate hypoxic and 9 severe hypoxic conditions were achieved from all rats in Group A1. A similar experimental paradigm was employed for rats in Group A2 and resulted in 27 control, 9 hypercapnic, and 9 moderate and 9 severe hypoxic conditions. After each experimental condition, five minutes were allowed for stabilization of animal’s physiology. In Group A1 (no imaging was performed), blood samples were concurrently obtained from the jugular vein (JV) and the superior sagittal sinus (SSS) at the end of each experimental condition. In Group A2, MR images were acquired and only JV blood samples were obtained immediately after imaging acquisition. SSS blood samples were not collected in Group A2 to avoid imaging artifacts induced by the surgical

procedures in accessing SSS. pO2, pCO2, pH and temperature of blood samples were obtained using a blood gas analyzer (Model 248, Bayer Corp). Measured pO_2 was first converted to human scales by using a rodent-to-human conversion factor of 0.694 and then was translated into O2Sat based on the oxygen dissociation curve after correcting for pH and temperature[13].

Group B included 22 MCAO and 9 sham operated rats. Surgical procedures for the intraluminal suture MCAO were similar to that previously described [14]. All animals were anesthetized with isoflurane and thermal stability (37±0.5°C) was maintained with a servo-controlled water pad connected to a rectal thermometer. A 4-0 nylon monofilament with heat-blunted tip was inserted through an arteriotomy of the common carotid artery (CCA). After acquiring baseline T2 weighted images, the suture was advanced 20–22 mm into the internal carotid artery to induce MCAO in-bore. Reperfusion was achieved 90 minutes post MCAO by withdrawing the suture from the origin of MCA/anterior cerebral artery to CCA. A similar surgical procedure was performed in the sham operated group without advancing the suture to occlude MCA.

Imaging Methods

All MR images were acquired on a Siemens 3T Allegra (Siemens Medical Systems, Erlangen, Germany), with a 4.3 cm custom birdcage volume coil (Nova Medical; Waltham, MA). The system was manually shimmed to minimize background magnetic field variation. A 2D multi-echo gradient echo/spin echo (MEGESE) sequence was utilized to estimate $O2Sat_{MR}$/MR_OEF[4]. In Group A2, MEGESE images were acquired once for each experimental condition, while in Group B, MEGESE was acquired sequentially every 15 minutes for 90 minutes after MCAO. Eight gradient echoes (GEs) prior to the spin echo (SE), and 19 GEs after the SE were acquired with a SE TE of 46.58 msec [4] and a TR of 1500 msec. All twenty-eight echoes were equally spaced with an inter-echo spacing of 2.5 msec. Field-of-view and matrix size were set to $45\times45mm^2$ and 64 × 64 sinc interpolated to 128 × 128, respectively, with a slice thickness of 1mm, achieving a spatial resolution of $0.7 \times 0.7 \times 1mm^3$ (nominal spatial resolution of $0.35 \times 0.35 \times 1\ mm^3$). In addition, a segmented EPI GE sequence was employed immediately prior to reperfusion for dynamic susceptibility contrast (DSC) perfusion measurements using Gd-DTPA in Group B. The imaging parameters were as follows: TR/TE=120/13 ms, an EPI factor of 15, and an identical resolution to that of MEGESE. The effective temporal resolution of the DSC was 0.48 sec and the total data acquisition time was 1 minute. Finally, T2-weighted (T2W) images were acquired pre and 24 hours after MCAO.

Parameter Estimation

Detailed descriptions for estimating $O2Sat_{MR}$ have been described previously [15]. In this study, similar approaches were utilized in both Groups A2 and B. Prior to any computation, a 3 × 3 averaging low pass filter was utilized to improve signal-to-noise. In Group B, MR_OEF was computed as $O2Sat_{art}$ - $O2Sat_{MRv}$ where $O2Sat_{art}$ was approximated as 1 during MCAO. An arterial input function was manually chosen in the MCA of the contralateral hemisphere and the singular value decomposition method was utilized to compute CBF [16]. MR_COMI was then calculated as the product of MR_OEF and CBF for Group B.

Data Analysis

Linear regression was performed for Group A1 to derive a relationship between $O2Sat_{SSS}$ and $O2Sat_{JV}$. Subsequently, this linear relationship was utilized to convert the experimentally measured $O2Sat_{JV}$ to $O2Sat_{SSS}$ in Group A2 so that a direct comparison could be made to MR-derived measures. In Group A2, two ROIs encompassing each hemisphere were used to obtain mean values of $O2Sat_{MRv}$. Linear regression was then performed between $O2Sat_{MRv}$ and $O2Sat_{JV}$ as well as the converted $O2Sat_{SSS}$. Tukey's test for multiple comparisons was utilized

to statistically compare the oxygen saturation between the MR measurements and blood gas oximetry at each cerebral oxygenation state.

In Group B, the acute and 24hrs T2W images from the same rats were registered by an affine method using FSL 3.2 (FMRIB, Oxford, UK). Four different ROIs were defined in the registered 24-hr T2W images. Specifically, the INFARCT ROI was manually delineated as the hyper-intense regions in the ipsilateral hemisphere. PERI ROI was manually defined as the peripheral region around T2-defined lesion without including ventricle in the ipsilateral hemisphere. The CONTRA ROI was manually outlined encompassing the entire contralateral hemisphere without ventricle. Finally, SHAM ROI was defined in the sham operated hemisphere. Voxels close to brain edge were carefully excluded in the definition of all ROIs to avoid potential confounds of non-brain regions. The median value of MR_COMI in the CONTRA ROI at each time point was utilized to normalize MR_COMI of the remaining ROIs at the same time point. The normalized MR_COMI (rMR_COMI) in each ROI from all rats were pooled together. A Tukey's test for multiple comparisons was utilized to statistically compare rMR_COMI from every ROI at each time point.

To determine the spatiotemporal evolution of ischemic lesions, two different analyses were performed 1) to examine if the rMR_COMI values in the ischemic lesions continued to decline, and 2) to examine if regions with severely depressed rMR_COMI grew over time. The former examination was achieved with histogram analysis by evaluating the temporal evolution of rMR_COMI of all ROIs at three histogram percentiles (25th, 50th and 75th percentiles). Linear regression was performed between the rMR_COMI values of the three percentiles and post MCAO time (in minutes) for all ROIs. A statistically negative slope ($r<0$, $P<0.05$) indicates a reduction in rMR_COMI values as a function of time. In addition, examination on the expansion or shrinkage of a region was achieved by counting the number of voxels (NumVoxels) in three different ranges of rMR_COMI (rMR_COMI ≤ 38%, 38%<rMR_COMI ≤ 70%, and rMR_COMI >70%) within the ipsilateral hemisphere at each time point. Linear regression was performed between NumVoxels and ischemia time (in minutes). A statistically positive slope ($r>0$, $p<0.05$) indicates an expansion or vice versa. In all the aforementioned linear regression, the ischemia time was chosen as the time at the center of each data acquisition interval.

Results

Manipulation of inhaled gas (control, hyperoxic hypercapnia, moderate, and severe hypoxia) led to statistically significant changes in blood oxygen saturation (Table 1, $P<0.05$). Similar $O2Sat_{MRv}$ (0.57 and 0.60) were obtained during the two successive control (room air) conditions (Figure 1b and 1d), demonstrating the consistency of our approach. As expected, moderate and severe hypoxia resulted in modest (Figure 1c, $O2Sat_{MRv}= 0.47$) and severe (Figure 1e, $O2Sat_{MRv}= 0.22$) global reductions of $O2Sat_{MRv}$, respectively. On the other hand, $O2Sat_{MRv}$ increased dramatically in the whole brain during hyperoxic hypercapnia (Figure 1f, $O2Sat_{MRv}=0.76$) when compared to the control state (Figure 1g, $O2Sat_{MRv}=0.67$).

$O2Sat_{JV}$ was consistently higher than $O2Sat_{SSS}$ (Figure 2a), as would be expected due to extracranial blood contributions to the JV blood samples. A highly linear relationship was observed between $O2Sat_{JV}$ and $O2Sat_{SSS}$ ($r=0.95$), suggesting that $O2Sat_{JV}$ can be used to reliably predict $O2Sat_{SSS}$ for rats in Group A2. Using this empirically determined relationship, $O2Sat_{MRv}$ was directly compared to the converted $O2Sat_{SSS}$. Highly linear relationships (Figure 2b) were obtained between $O2Sat_{MRv}$ vs. $O2Sat_{JV}$ ($r=0.94$), and $O2Sat_{MRv}$ vs. $O2Sat_{SSS}$ ($r=0.94$). As expected, the linear regression between $O2Sat_{JV}$ and $O2Sat_{MRv}$ is above the line of identity (Figure 2b) and $O2Sat_{JV}$ is significantly higher than $O2Sat_{MRv}$ during control and hyperoxic hypercapnia ($P<0.05$, Figure 2c). On the other hand, the linear regression

between $O2Sat_{MRv}$ and $O2Sat_{SSS}$ is similar to the line of identity (Figure 2b). These results suggest that MR measured oxygen saturation is accurate compared to gold standard blood oximetry measurements. The group mean and standard deviation of $O2Sat_{JV}$, $O2Sat_{SSS}$, and $O2Sat_{MRv}$ under each experimental condition were summarized in Figure 2c. Note that the mean control MR_OEF (42%=100%−58%) (Figure 2c) is in agreement with PET OEF measurements under normal conditions [17, 18].

Using this MR approach to derive MR_COMI (CBF × OEF), we serially imaged a group of rats subjected to focal ischemia. Four representative rats are shown in Figure 3, exhibiting decreasing levels of ischemia (rows a to c) and a sham operated control (row d). The most severely ischemic rat (row a**)** demonstrated a large region with markedly reduced rMR_COMI shortly after MCAO, which remained low throughout the entire duration of ischemia. A moderately ischemic rat (row b) demonstrated a region of depressed rMR_COMI that progressively grew larger with time (marked by arrow). In both rats, regions of severely reduced rMR_COMI appeared to be predictive of the final T2-defined lesion. A rat with mild ischemia (row c**)** demonstrated modest reductions in rMR_COMI throughout the entire period of ischemia, and an infarct did not develop in the follow-up scan. A sham-operative rat (row d**)** showed no apparent change in rMR_COMI and did not develop an infarct. These results suggest that rMR_COMI can be used to delineate different severities of ischemia.

rMR_COMI in INFARCT (the final T2W infarct region) was significantly lower than all other ROIs ($P<0.05$) at each time point (Fig. 4a). In addition, PERI (the peripheral region around INFARCT in the ipsilateral hemisphere) showed moderately but significantly lower rMR_COMI ($P<0.05$) than SHAM and CONTRA. Finally, the SHAM and CONTRA exhibited similar rMR_COMI values ($P>0.05$).

To determine the temporal evolution of rMR_COMI, all quartiles of rMR_COMI histogram were examined within each ROI. In the INFARCT ROI, the 75th percentile of the rMR_COMI value had the greatest reduction ($P<0.05$) followed by the 50th percentile ($P<0.05$), while the changes at the 25th percentile were not significant ($P=0.12$) (Figure 4, a and b). In contrast, the remaining three ROIs (PERI, CONTRA, and SHAM) did not demonstrate any significant change in rMR_COMI with time (data not shown).

An interesting characteristic of the rMR_COMI frequency histograms is that these histograms exhibited two major peaks regardless of elapsed ischemia time (Figure 4c). The peak centered at an rMR_COMI value of 0.15 appeared to be stable throughout the entire ischemic period; however, the second peak exhibited a time-dependent decline to lower rMR_COMI values. In the ipsilateral hemisphere, NumVoxels of ‘rMR_COMI ≤ 38%’ increased significantly ($P<0.05$), and NumVoxels of ‘38% < rMR_COMI ≤ 70%’ decreased significantly ($P<0.05$) over time (Figure 4d). This observation suggested that more voxels have migrated into the severely depressed rMR_COMI territory as lesion progressed. Finally, temporal changes of NumVoxels of ‘rMR_COMI >70%’ were not significant ($P=0.11$).

Discussion

During cerebral ischemic insults, alterations of cerebral hemodynamics and metabolism are highly dynamic. After the onset of cerebral ischemia, OEF is elevated in an effort to compensate for the reduced CBF and maintain a stable $CMRO_2$ so as to preserve neuronal function and/or cellular integrity [3, 19–22]. When the reduction of CBF exhausts the compensatory capability of OEF, $CMRO_2$ will decrease. Therefore, a reduction of $CMRO_2$ may be a more specific marker than that of OEF or CBF in delineating tissue viability since CBF threshold for irreversible injury is highly time dependent[22]. Moreover, OEF may have biphasic behavior during ischemia, making it difficult to define a single viability threshold [2, 19]. Although

quantitative measures of $CMRO_2$ can be derived using PET, an MR approach may greatly facilitate routine clinical applications.

With experimental hypoxia and hyperoxic hypercapnia, a wide and physiologically relevant range of cerebral blood oxygenation was achieved, allowing validation of MR_OEF against gold-standard blood gas oximetry measures. Because of extracranial contributions to JV blood, the oxygen saturation in the JV is higher than that of cerebral venous blood [23, 24]. Ideally, the $O2Sat_{MRv}$ should be directly compared with the experimentally measured $O2Sat_{SSS}$ [23–25]. However, surgical procedures to access SSS blood can induce susceptibility artifacts in MR images, making a direct comparison between $O2Sat_{MRv}$ and $O2Sat_{SSS}$ in the same animal impossible. To overcome this problem, a separate calibration was utilized to empirically obtain the relationship between $O2Sat_{JV}$ and $O2Sat_{SSS}$. This relationship allowed a conversion of $O2Sat_{JV}$ to $O2Sat_{SSS}$ when direct measurements of $O2Sat_{SSS}$ were not possible. Using this conversion, a highly linear relationship between $O2Sat_{MRv}$ and the converted $O2Sat_{sss}$ was obtained (r=0.94) with a slope of 0.97 and an intercept of 0.021, suggesting that an accurate measure of cerebral blood oxygenation can be obtained.

In this study, the imaging resolution was $0.7 \times 0.7 \times 1mm^3$ and sinc interpolated to a nominal spatial resolution of $0.35 \times 0.35 \times 1\ mm^3$. A 3*3 filter applied on the extrapolated images lead to a spatial resolution of $1.05 \times 1.05 \times 1mm^3$ for the MR_COMI images. Similar to the reported results from PET [10, 18], O2Sat is quite homogenous in both gray matter and white matter. It may be possible that spatial variation of O2Sat exist between different tissue types. However, our method and PET based approaches might not have the resolution and sensitivity to detect it.

With the ability to obtain accurate measures of MR_OEF in vivo, MR_COMI was obtained in a transient MCAO rat model to determine its spatiotemporal evolution during acute ischemia. In this study, an intraluminal suture MCAO model was chosen to induce cerebral ischemia. Compared to the three vessel ligation stroke model, the intraluminal suture model is known to induce more variable ischemic injuries [26, 27]. As shown in Figure 3, varying degrees of injury were induced and permitted the evaluation of MR_COMI under different situations.

As demonstrated by Figure 4a, an rMR_COMI of 38% (dashed line, Figure 4a) appears to delineate infarct from peri region. In a human study, Powers et al studied 50 patients with different degrees of cerebral ischemia and demonstrated that brain tissue might be viable with a $CMRO_2$ greater than 37–39% of the normal value. In addition, $CMRO_2$ thresholds ranging from 40% to 45% to separate irreversible injury have been reported in primates using PET [1, 2, 28] Consistent with these results, the proposed rMR_COMI method may hold promise in predicting tissue outcome. The putative rMR_COMI threshold (38%) was utilized to delineate regions with extensive rMR_COMI impairment in Figure 3. In Fig. 3a, a severely injured region was observed shortly after MCAO. The spatiotemporal evolution of the ischemic lesion in this rat is not apparent. A plausible reason is that this ischemic tissue might evolve very quickly and reached a low oxygen metabolic state early into the MCAO. On the other hand, a moderately injured tissue as in Figure 3b, clearly showed an expansion of lesion over time. Figure 3 shows only representative images. Quantitative measures to study spatiotemporal evolution of lesion from all animals were summarized in Figure 4.

In summary, three major findings regarding the spatiotemporal evolution of ischemic rMR_COMI are shown in Fig. 4b – 4d. Specifically, the values of rMR_COMI at both 75^{th} and 50^{th} percentiles within the ischemic lesion declined significantly over time (Figure 4b). Second, the histogram analysis (Fig. 4c) reveals the continuing reduction of rMR_COMI as demonstrated by the increased population towards to the lower rMR_COMI as the duration of MCAO increased. This finding is consistent with the results reported by Shen et al using a

DWI/PWI defined lesion volume in a similar transient MCAO rat model [29]. Finally, the number of voxels exhibiting a severe reduction of rMR_COMI (<38% of the contralateral hemisphere) continued to increase significantly as MCAO duration increased, consistently with that shown in Figure 3 (2nd row). Conversely, the number of voxels with a moderate reduction of rMR_COMI (38%<rMR_COMI<70% of the contralateral hemisphere) continued to reduce significantly, indicating that more voxels are recruited into regions with an rMR_COMI less than 38%. This finding is consistent with the histogram results shown in Fig. 4c.

Moreover, our data suggested that the spatiotemporal evolution of rMR_COMI values had different courses depending on the severity of tissue injury. The most severely reduced rMR_COMI values (25th percentile), remains rather stable, while modest decreased rMR_COMI values (the 50th and 75th percentiles) continued to decline. An MR perfusion and diffusion imaging study reported a similar finding[29]. In this study, ischemic 'core' that was already identified at their earliest acquisition time point (30 minutes post MCAO) remained stable throughout the MCAO duration, while the presumed penumbra continued to be recruited into the core regions. It has been demonstrated that the fate of tissue depends on the severity of injury, and tissue may become necrotic as early as 15 minutes after ischemia with low flow [30, 31]. Consistent with these reports, our results demonstrated that progression of rMR_COMI values might be more apparent in lesions with undetermined fate (e.g. penumbra), while evolution of rMR_COMI values in already necrotic regions might be minimal.

In the current study, only the acute spatiotemporal evolution of the ischemic lesion was studied. While it is plausible that ischemic lesions continue to evolve beyond 24hrs, particularly in stroke patients, the lesion evolves much faster in MCAO rats. Using a similar MCAO rat model, Memezawa et al have reported that infarct size increased progressively with increasing occlusion time and the 120–180 minutes occlusion infarcts were as extensive as those of permanent MCAO.[31] In addition, it has been suggested that lesion progression is species and models dependent [30, 31]. In MCAO rat model, 24 hr–72 hr have been utilized widely as the end point in the determination of final infarct volume[29, 32]. It has been suggested that no substantial postischemic mcrovascular hupoperfusion was shown after 24 and 72 hours in a rat ischemia model [32]. The delay neuronal death after 24 hours post MCAO might be caused by other mechanisms including accumulation of calcium, apoptosis, inhibition of cellular protein synthesis. In our study, we only focus on evaluating acute lesion evolution with a future goal to obtain information related to ischemic tissue viability. The capability of delineating penumbra from core will potentially facilitate patient selection for tissue plasminogen activator (tPA) treatment during acute phase.

DSC method was employed to obtain CBF in this study. Since the contrast agent induces MR signal alteration similar to that of deoxyhemoglobin, estimates of MR_OEF may be confounded in the presence of contrast. To avoid this problem, CBF was only acquired once prior to reperfusion. CBF was assumed to remain unchanged throughout the course of this surgically induced MCAO. An alternative approach might be to use arterial spin labeling (ASL) to measure CBF [33]. However, long data acquisition times are needed to achieve sufficient SNR using ASL, making it difficult to rapidly characterize the temporal alterations of cerebral oxygen metabolism during acute ischemia. Nevertheless, it has been demonstrated that CBF remains stable during MCAO in a similar rat stroke model [29]. Therefore, although CBF was only obtained once for the calculation of MR_COMI, it should not affect the findings of our studies.

CONCLUSION

With experimental hypoxia and hyperoxic hypercapnia, we have demonstrated that an accurate measure of MR_OEF can be achieved across a wide range of cerebral blood oxygenation.

MR_COMI, a measure closely related to $CMRO_2$, can be obtained by combining MR_OEF and CBF. We have demonstrated that rMR_COMI values within the ischemic territory declined with time, concomitant with an increase in the area of severely impaired oxygen metabolism in ischemic rats. In addition, significantly lower rMR_COMI was observed in tissue that progressed to infarction. An rMR_COMI value below 38% appeared to separate the final infarction from surviving tissue. In summary, the proposed MR_COMI method provides complementary information to other widely used methods, such as perfusion/diffusion MR imaging. A multi-modal approach to non-invasively assess tissue viability may have profound clinical implications for the management of acute stroke patients in the future.

Acknowledgments

This study was supported by grants from National Institute of Health (NIH R01 NS37312, NIH S10 RR017212) and American Heart Association (AHA 0730321N). We thank Dr. Jin-Moo Lee for his valuable discussion and review of this manuscript.

Abbrevations

JV
: jugular vein

SSS
: superior sagittal sinus

O2Sat
: oxygen saturation

$O2Sat_{MRV}$
: MR measured venous cerebral blood oxygen saturation

$O2Sat_{JV}$
: jugular veous blood oxygen saturation obtained from blood gas oximetry

$O2Sat_{SSS}$
: superior sagittal sinus blood oxygen saturation obtained from blood gas oximetry

$O2Sat_{FA}$
: femoral arterial blood oxygen saturation obtained from blood gas oximetry

MCAO
: middle cerebral artery occlusion

CBF
: cerebral blood flow

MR_OEF
: MR measured oxygen extraction fraction

MR_COMI
: MR cerebral oxygen metabolic index

References

1. Frykholm P, Andersson JL, Valtysson J, Silander HC, Hillered L, Persson L, Olsson Y, Yu WR, Westerberg G, Watanabe Y, Langstrom B, Enblad P. A metabolic threshold of irreversible ischemia demonstrated by pet in a middle cerebral artery occlusion-reperfusion primate model. Acta Neurol Scand 2000;102:18–26. [PubMed: 10893058]

2. Young AR, Sette G, Touzani O, Rioux P, Derlon JM, MacKenzie ET, Baron JC. Relationships between high oxygen extraction fraction in the acute stage and final infarction in reversible middle cerebral artery occlusion: An investigation in anesthetized baboons with positron emission tomography. J Cereb Blood Flow Metab 1996;16:1176–1188. [PubMed: 8898690]
3. Powers WJ, Grubb RL Jr, Darriet D, Raichle ME. Cerebral blood flow and cerebral metabolic rate of oxygen requirements for cerebral function and viability in humans. J Cereb Blood Flow Metab 1985;5:600–608. [PubMed: 3877067]
4. An H, Lin W. Quantitative measurements of cerebral blood oxygen saturation using magnetic resonance imaging. Journal of Cerebral Blood Flow & Metabolism 2000;20:1225–1236. [PubMed: 10950383]
5. An H, Lin W. Cerebral oxygen extraction fraction and cerebral venous blood volume measurements using magnetic resonance imaging: Effects of magnetic field variation. Magnetic Resonance in Medicine 2001;47:958–966. [PubMed: 11979575]
6. An H, Lin W. Impact of intravascular signal on quantitative measures of cerebral oxygen extraction and blood volume under normo- and hypercapnic conditions using an asymmetric spin echo approach. Magn Reson Med 2003;50:708–716. [PubMed: 14523956]
7. An H, Lin W, Celik A, Lee YZ. Quantitative measurements of cerebral metabolic rate of oxygen utilization using mri: A volunteer study. NMR Biomed 2001;14:441–447. [PubMed: 11746936]
8. Lee JM, Vo KD, An H, Celik A, Lee Y, Hsu CY, Lin W. Magnetic resonance cerebral metabolic rate of oxygen utilization in hyperacute stroke patients. Ann Neurol 2003;53:227–232. [PubMed: 12557290]
9. Rhodes CG, Lenzi GL, Frackowiak RS, Jones T, Pozzilli C. Measurement of cbf and cmro2 using the continuous inhalation of c15o2 and 15o. Experimental validation using co2 reactivity in the anaesthetised dog. J Neurol Sci 1981;50:381–389. [PubMed: 6790677]
10. Ashkanian M, Borghammer P, Gjedde A, Ostergaard L, Vafaee M. Improvement of brain tissue oxygenation by inhalation of carbogen. Neuroscience 2008;156:932–938. [PubMed: 18786619]
11. Sedlacik J, Kutschbach C, Rauscher A, Deistung A, Reichenbach JR. Investigation of the influence of carbon dioxide concentrations on cerebral physiology by susceptibility-weighted magnetic resonance imaging (swi). Neuroimage 2008;43:36–43. [PubMed: 18678260]
12. Rijpkema M, Schuuring J, Bernsen PL, Bernsen HJ, Kaanders JH, van der Kogel AJ, Heerschap A. Bold mri response to hypercapnic hyperoxia in patients with meningiomas: Correlation with gadolinium-dtpa uptake rate. Magn Reson Imaging 2004;22:761–767. [PubMed: 15234444]
13. Hall FG. Minimal utilizable oxygen and the oxygen dissociation curve of blood of rodents. J Appl Physiol 1966;21:375–378. [PubMed: 5934438]
14. Longa EZ, Weinstein PR, Carlson S, Cummins R. Reversible middle cerebral artery occlusion without craniectomy in rats. Stroke 1989;20:84–91. [PubMed: 2643202]
15. Yablonskiy DA, Haacke EM. Theory of nmr signal behavior in magnetically inhomogeneous tissues: The static dephasing regime. Magnetic Resonance in Medicine 1994;32:749–763. [PubMed: 7869897]
16. Ostergaard L, Weisskoff RM, Chesler DA, Gyldensted C, Rosen BR. High resolution measurement of cerebral blood flow using intravascular tracer bolus passages. Part i: Mathematical approach and statistical analysis. Magn Reson Med 1996;36:715–725. [PubMed: 8916022]
17. Yamauchi H, Fukuyama H, Nagahama Y, Nabatame H, Nakamura K, Yamamoto Y, Yonekura Y, Konishi J, Kimura J. Evidence of misery perfusion and risk for recurrent stroke in major cerebral arterial occlusive diseases from pet. Journal of Neurology, Neurosurgery & Psychiatry 1996;61:18–25.
18. Nakane H, Ibayashi S, Fujii K, Sadoshima S, Irie K, Kitazono T, Fujishima M. Cerebral blood flow and metabolism in patients with silent brain infarction: Occult misery perfusion in the cerebral cortex. Journal of Neurology, Neurosurgery & Psychiatry 1998;65:317–321.
19. Heiss WD, Graf R, Wienhard K, Lottgen J, Saito R, Fujita T, Rosner G, Wagner R. Dynamic penumbra demonstrated by sequential multitracer pet after middle cerebral artery occlusion in cats. J Cereb Blood Flow Metab 1994;14:892–902. [PubMed: 7929654]

20. Heiss WD, Huber M, Fink GR, Herholz K, Pietrzyk U, Wagner R, Wienhard K. Progressive derangement of periinfarct viable tissue in ischemic stroke. J Cereb Blood Flow Metab 1992;12:193–203. [PubMed: 1548292]
21. Pappata S, Fiorelli M, Rommel T, Hartmann A, Dettmers C, Yamaguchi T, Chabriat H, Poline JB, Crouzel C, Di Giamberardino L, et al. Pet study of changes in local brain hemodynamics and oxygen metabolism after unilateral middle cerebral artery occlusion in baboons. J Cereb Blood Flow Metab 1993;13:416–424. [PubMed: 8478400]
22. Jones TH, Morawetz RB, Crowell RM, Marcoux FW, FitzGibbon SJ, DeGirolami U, Ojemann RG. Thresholds of focal cerebral ischemia in awake monkeys. J Neurosurg 1981;54:773–782. [PubMed: 7241187]
23. Altman DI, Lich LL, Powers WJ. Brief inhalation method to measure cerebral oxygen extraction fraction with pet: Accuracy determination under pathologic conditions. J Nucl Med 1991;32:1738–1741. [PubMed: 1880576]
24. Hattori N, Bergsneider M, Wu HM, Glenn TC, Vespa PM, Hovda DA, Phelps ME, Huang SC. Accuracy of a method using short inhalation of (15)o-o(2) for measuring cerebral oxygen extraction fraction with pet in healthy humans. J Nucl Med 2004;45:765–770. [PubMed: 15136624]
25. Ogawa S, Lee TM, Barrere B. The sensitivity of magnetic resonance image signals of a rat brain to changes in the cerebral venous blood oxygenation. Magn Reson Med 1993;29:205–210. [PubMed: 8429784]
26. Schmid-Elsaesser R, Zausinger S, Hungerhuber E, Baethmann A, Reulen HJ. A critical reevaluation of the intraluminal thread model of focal cerebral ischemia: Evidence of inadvertent premature reperfusion and subarachnoid hemorrhage in rats by laser-doppler flowmetry. Stroke 1998;29:2162–2170. [PubMed: 9756599]
27. Xi GM, Wang HQ, He GH, Huang CF, Wei GY. Evaluation of murine models of permanent focal cerebral ischemia. Chin Med J (Engl) 2004;117:389–394. [PubMed: 15043779]
28. Touzani O, Young AR, Derlon JM, Baron JC, MacKenzie ET. Progressive impairment of brain oxidative metabolism reversed by reperfusion following middle cerebral artery occlusion in anaesthetized baboons. Brain Res 1997;767:17–25. [PubMed: 9365011]
29. Shen Q, Meng X, Fisher M, Sotak CH, Duong TQ. Pixel-by-pixel spatiotemporal progression of focal ischemia derived using quantitative perfusion and diffusion imaging. J Cereb Blood Flow Metab 2003;23:1479–1488. [PubMed: 14663344]
30. Heiss WD, Graf R. The ischemic penumbra. Curr Opin Neurol 1994;7:11–19. [PubMed: 8173671]
31. Memezawa H, Smith ML, Siesjo BK. Penumbral tissues salvaged by reperfusion following middle cerebral artery occlusion in rats. Stroke 1992;23:552–559. [PubMed: 1561688]
32. Li F, Han SS, Tatlisumak T, Liu KF, Garcia JH, Sotak CH, Fisher M. Reversal of acute apparent diffusion coefficient abnormalities and delayed neuronal death following transient focal cerebral ischemia in rats. Ann Neurol 1999;46:333–342. [PubMed: 10482264]
33. Wang J, Zhang Y, Wolf RL, Roc AC, Alsop DC, Detre JA. Amplitude-modulated continuous arterial spin-labeling 3.0-t perfusion mr imaging with a single coil: Feasibility study. Radiology 2005;235:218–228. [PubMed: 15716390]

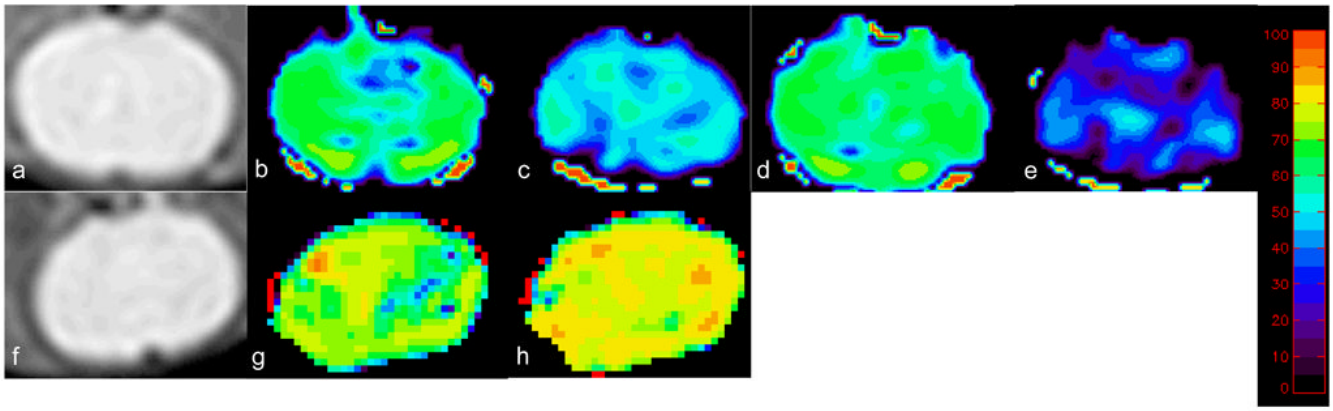

Figure 1.

Spin echo image from a representative rat (a) and $O2Sat_{MRv}$ maps under control condition (b), followed by moderate hypoxia (c), followed by another control condition (d), followed by severe hypoxia (e). Spin echo image (f) and $O2Sat_{MRv}$ maps from a separate rat undergoing control condition (g) followed by hyperoxic hypercapnia (h). The color bar represents the scale for blood oxygenation (0 to 100%).

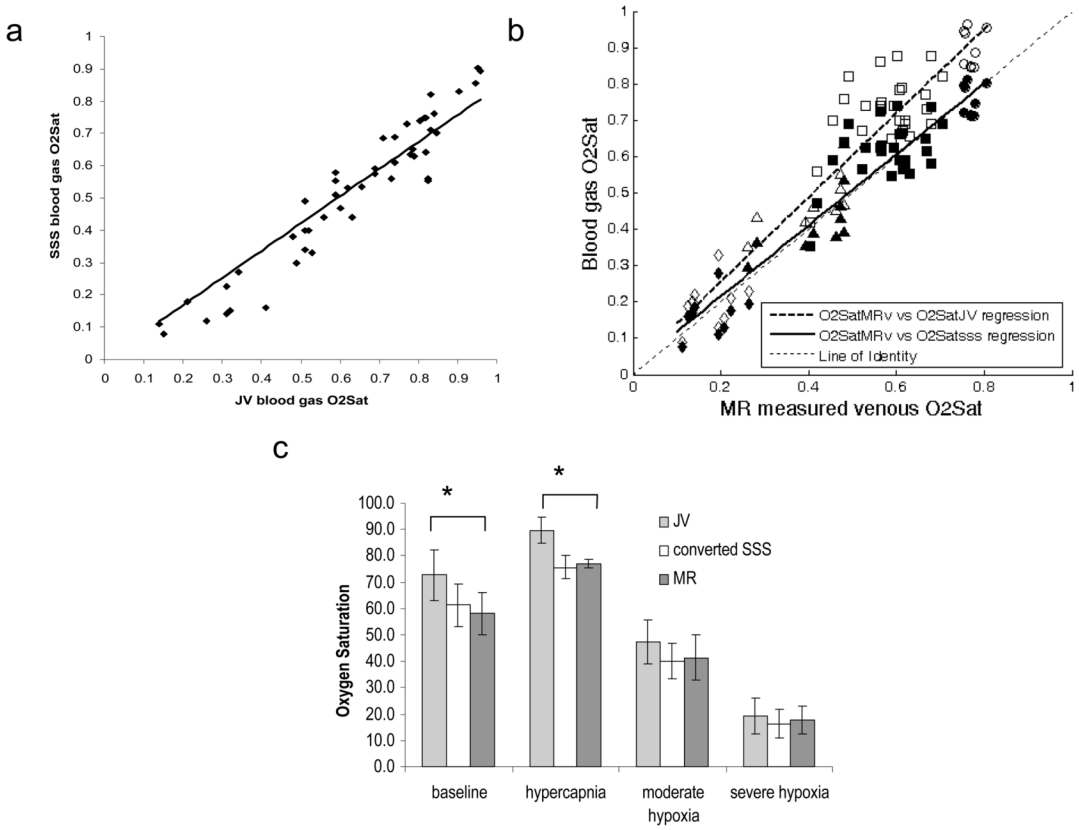

Figure 2.

(a) Linear regression between the experimentally measured $O2Sat_{JV}$ vs. ($O_2Sat_{SSS} = 0.8424 \cdot O_2Sat_{JV}$; r=0.95); (b) Plot of $O2Sat_{MRv}$ vs. $O2Sat_{JV}$ (open symbols) and the converted $O2Sat_{sss}$ (closed symbols) during control (squares), hyperoxic hypercapnia (circles), moderate hypoxia (triangles) and severe hypoxia (diamonds). Linear regression between $O2Sat_{MRv}$ vs $O2Sat_{JV}$ ($O_2Sat_{JV} = 1.159 \cdot O_2Sat_{MRv}$; r=0.94, dashed line) and $O2Sat_{MRv}$ vs $O2Sat_{SSS}$ ($O_2Sat_{SSS} = 0.9763 \cdot O_2Sat_{MRv} + 0.021$; r=0.94; solid line) were plotted together with a line of identity (dotted line). (c) Mean and standard deviation of $O2Sat_{JV}$ (0.73±0.10, 0.90±0.05, 0.47±0.08 and 0.20±0.07), converted $O2Sat_{SSS}$ (0.61±0.08, 0.76±0.04, 0.40±0.07 and 0.16 ±0.06) and $O2Sat_{MRv}$ (0.58±0.08, 0.77±0.05, 0.41±0.09 and 0.18±0.05) under control, hyperoxic hypercapnia, moderate, and severe hypoxia (from left to right). * P<0.05.

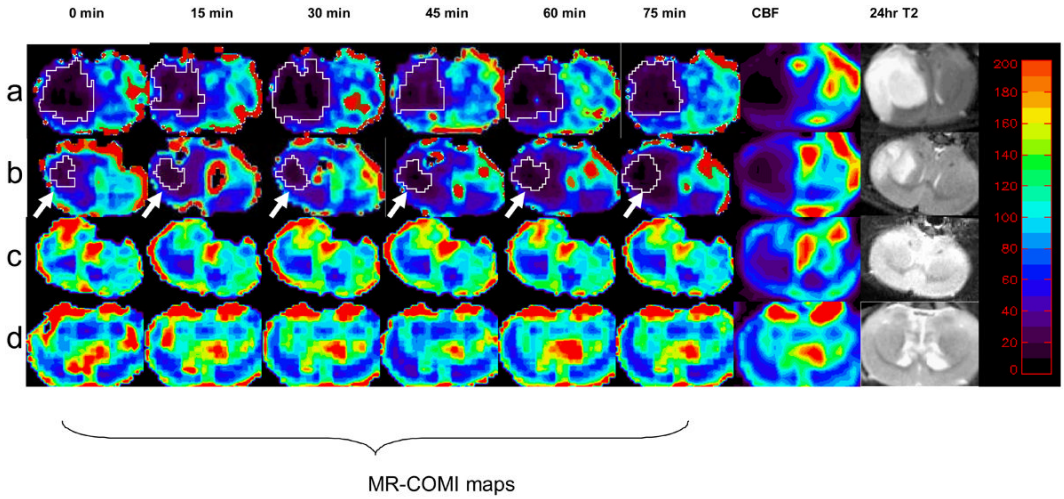

Figure 3.

rMR_COMI (first 6 columns), rCBF (7th column) and 24-hr T2 maps (the last column) from four representative rats. The starting time (min) of each data acquisition is labeled at the top of the MR_COMI panel. Contour outlines ischemic lesions with an rMR_COMI<38%. The color bar shows a range from 0 to 200%.

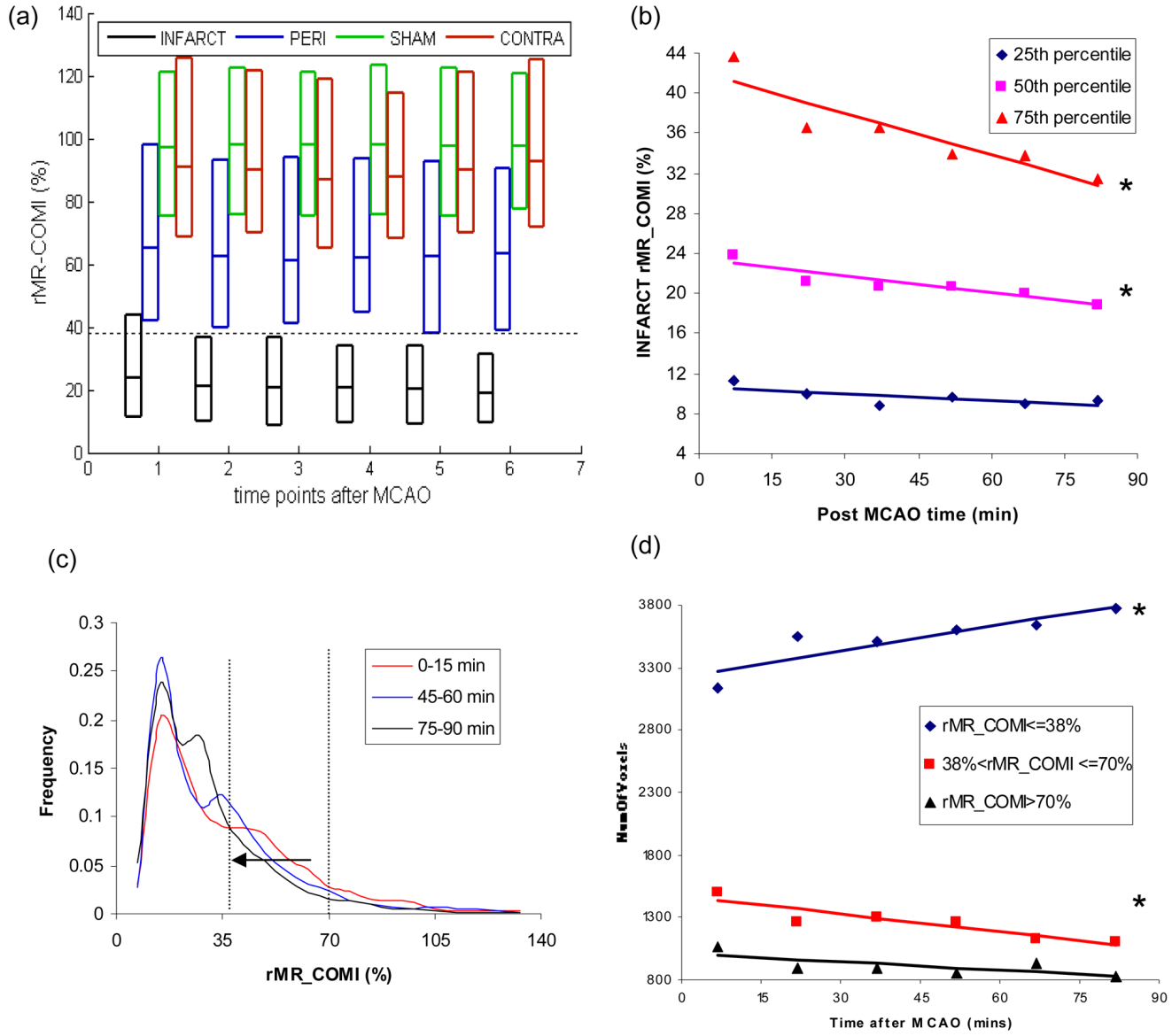

Figure 4.

(a) Three quartiles of the histogram for INFARCT, PERI, SHAM, and CONTRA at each time point. The bottom, middle and upper lines of the boxplot represent the 25th, 50th and 75th percentile of the histogram. A dotted line was drawn to show rMR_COMI value equivalent to 38% of the contralateral side; (b) Linear regression between rMR_COMI and ischemia time (T) for the 75th percentile (rMR_COMI=−0.1376T+42.088, r=−0.91, P<0.05), 50th percentile (rMR_COMI =−0.0545T+23.33, r=−0.92, P<0.05), and 25th percentile (rMR_COMI= −0.0224T+10.66, r=−0.70, P=0.12) of the histogram in INFARCT; (c) Histograms of the INFARCT ROI acquired at three time points (0–15, 45–60 and 75–90 minutes) with vertical dotted lines to show rMR_COMI value of 38% and 70%; (d) Linear regression between ischemia time (T) and NumVoxels of ‘rMR_COMI 38%’ (NumVoxels=6.886T+3227.1, r=0.89, P<0.05), ‘38%<rMR_COMI<=70%’ (NumVoxels=−4.747T+1473.2, r=−0.92, P<0.05) and rMR_COMI>70% (NumVoxels=−2.145T+1008.4, r=−0.7141, P=0.11). * P<0.05.

Table 1

Physiological parameters, including pH, pCO2, pO2 and blood oxygen saturation (O2Sat).

			pH	pCO2	pO2	O2Sat (%)
Calibration group	Control (n=24)	FA	7.44±0.06	36.5±4.8	116.9±36.2	93.4±5.6
		JV	7.42±0.07	39.8±5.0	57.8±8.4	74.1±9.6
		SSS	7.41±0.06	43.6±4.2	47.0±6.5	62.9±9.2
	Hyperoxic hypercapnia (n=5)	FA	7.35±0.03*	51.3±3.6*	398.5±8.6*	99.7±0.1
		JV	7.33±0.03	54.0±4.1*	111.5±24.2*	91.8±5.4*
		SSS	7.31±0.03*	58.3±4.5*	86.2±8.8*	86.1±3.7*
	Moderate hypoxia (n=10)	FA	7.46±0.06	33.6±2.5	55.4±12.8*	73.6±8.4*
		JV	7.43±0.06	37.6±4.0	40.0±3.8*	54.5±4.7*
		SSS	7.41±0.06	42.7±3.2	32.1±4.5*	41.2±7.1*
	Severe hypoxia (n=9)	FA	7.46±0.08	27.2±4.0*	35.6±6.2*	49.7±9.2*
		JV	7.41±0.09	34.0±5.3*	23.6±6.1*	27.2±9.0*
		SSS	7.38±0.08	37.3±4.5*	16.7±5.8*	15.9±5.9*
Imaging group	Control (n=27)	FA	7.46±0.05	36.7±4.9	92.5±21.8	90.7±5.4
		JV	7.46±0.04	37.2±4.0	53.2±10.6	71.9±10.7
	Hyperoxic hypercapnia (n=9)	FA	7.29±0.03*	56.7±6.2*	397.5±35.9*	99.6±0.2*
		JV	7.27±0.02*	64.4±4.9*	111.0±24.0*	90.5±4.7*
	Moderate hypoxia (n=9)	FA	7.51±0.03*	30.7±2.7*	42.5±4.5*	63.2±7.4*
		JV	7.48±0.03*	33.1±2.3*	33.4±4.3*	47.4±8.2*
	Severe hypoxia (n=9)	FA	7.40±0.05*	24.9±3.7*	32.0±2.0*	39.7±2.1*
		JV	7.37±0.06*	31.7±4.2*	18.9±4.0*	19.5±6.8*

* P<0.05 when compared to the control. n indicates the number of experimental conditions.